A Photochemical Method To Map Ethidium Bromide Binding Sites on DNA: Application to a Bent DNA Fragment†

Girija Krishnamurthy, Thomas Polte, Thomas Rooney, and Michael E. Hogan*

Center for Biotechnology, Baylor College of Medicine, The Woodlands, Texas 77381, and Department of Biology, Princeton University, Princeton, New Jersey 08544

Received July 27, 1989; Revised Manuscript Received September 13, 1989

ABSTRACT: It is shown that, when irradiated in the visible, ethidium bromide (EB) engages in direct photochemistry with its DNA binding site. At the photochemical end point, an average of one single-strand break is produced per bound EB molecule in a reaction which also bleaches the dye chromophore. Using high-resolution electrophoresis, we have mapped the distribution of EB photocleavage sites on DNA, at one-base resolution. It is argued that because the photocleavage is stoichiometric, the resulting pattern is similar to, if not identical with, the local distribution of EB binding affinity. When interpreted in the context of the extensive thermodynamic and structural data which are available for EB, a binding distribution of that kind can be used to infer details of DNA structure variation within the underlying helix. As a first application of the method, we have used EB to probe the structure of a 265 bp fragment of DNA, which had been described as being bent as the result of a periodic array of oligo(A) segments [Kitchin et al. (1986) *J. Biol. Chem. 261*, 11302]. The EB mapping data provide evidence that the oligo(A) elements in this fragment assume a local secondary structure which is different than that assumed by isolated ApA nearest neighbors and that the ends of the oligo(A) elements comprise a junctional domain with EB binding properties which differ from those of the oligo(A) element or of random-sequence DNA.

It is now generally agreed that DNA secondary structure can vary as a function of sequence. As predicted by 30 years of biophysical analysis, statistically random sequences assume a conformation which is close to the canonical B form under ordinary conditions of salt, hydration, and temperature (Leslie & Arnott, 1980). However, in regions where DNA sequence is nonrandom, a helix can relax into a secondary structure which is distinctly different from its surroundings.

Enzymatic and chemical probes of DNA structure variation have been developed to augment the physical methods: S1 nuclease (Felsenfeld, 1986); DNase I (Drew & Travers, 1984) aldehydes (Kowhi-Shigematsu et al., 1983); hydroxide radical (Burkoff & Tullius, 1987); diethyl pyrocarbonate (Johnston & Rich, 1985); and so on. Photochemical probes of structure variation have been especially useful, including ruthinium chelates (Wei & Barton, 1988), cobalt chelates (Muller et al., 1987), eosin analogues and methylene blue (Hogan et al., 1987), and pyrene derivatives (Boles & Hogan, 1984). The goal of the work described in this paper is to develop a new tool for this kind of microscopic structure analysis.

Ethidium bromide (EB) intercalation into a DNA helix is one of the best understood ligand–substrate interactions, resulting in 26° of twist reduction and local unstacking of the base planes (Saenger, 1984). We have reasoned that the EB binding process is so well understood that, if a method were developed to map the distribution of EB binding sites directly, it would be possible to interpret local variation of EB binding specificity in the context of usefully detailed structure models. For example, a domain which displays local reduction of helix twist or base stacking might be particularly attractive as a binding site (i.e., models of the "lock and key" type) as would a domain which, although undistinguished at the outset, more readily accommodates subsequent twist or stacking change in the bound complex (a model of the "induced fit" type).

Most particularly, because EB shows a very modest nearest-neighbor preference when binding to a random B-DNA helix (Kastrup et al., 1978; Baguley & Falkenhaug, 1978), observation of significant local variation of EB affinity may be prima facie evidence for local variation of the physical properties of the DNA binding site.

It has been known for some time that when irradiated in the visible, ethidium bromide engages in photochemistry which will cleave DNA (Deniss & Morgan, 1975). Building upon that observation, we describe here a photochemical method to map EB binding sites on DNA. On the basis of kinetic and mechanistic analysis of the process, we show that, under standard conditions of analysis, EB photocleavage can be driven to an end point at which the helix is cleaved once at the binding site in a reaction which is coupled to EB bleaching. We argue that as a consequence of that apparently simple reaction, the EB photocleavage distribution becomes similar to, if not identical with, the distribution of EB binding affinity within the region of interest, thereby simplifying analysis of the data in terms of discrete structural models.

Results and Discussion

Kinetics and Mechanism of EB Photocleavage. To study the kinetics and stoichiometry of EB-mediated photochemistry, complexes with a random-sequence 146 bp chicken DNA fragment were irradiated with the 514-nm output of an Ar^+ ion laser (see legend to Figure 1). Irradiated samples, along with untreated controls, were then analyzed by denaturing electrophoresis. Those kinetics are displayed in Figure 1A. The photocleavage reaction is exponential and plateaus at a limiting value near one cleavage per bound ethidium equivalent, suggesting that at the photochemical end point exactly one single-strand break is produced per bound EB. Under

† This work was supported by a grant to M.E.H. from the NCI.

* To whom correspondence should be addressed at the Center for Biotechnology, Baylor College of Medicine, 4000 Research Forest Dr., The Woodlands, TX 77381.

0006-2960/90/0429-981$02.50/0

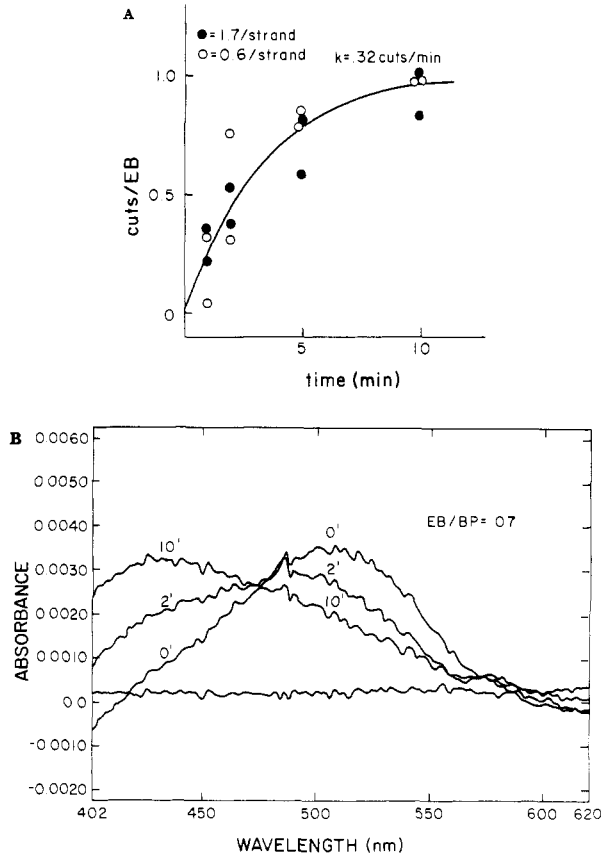

FIGURE 1: Ethidium-mediated DNA photochemistry. (A) EB photocleavage kinetics. 146 bp DNA fragments were isolated from chicken erythrocyte nucleosomes, as described elsewhere (Wang et al., 1982). EB was added to a bound density of either 0.6 or 1.7 EB/strand and irradiated in a 5-μL glass microcuvette. Temperature was controlled with a stream of argon. The standard buffer from photocleavage chemistry was 10 mM Tris-HCl and 1 mM Na_2EDTA, pH 7.8. DNA concentration was held constant at 5×10^{-4} M bp to ensure that added EB was bound to completion. The light source was an Ar^+ ion laser (Spectra-Physics) tuned to 514 nm at 2.5 W/cm^2. The doubled output (532 nm) of a pulsed Nd/YAG laser was employed in some experiments, but the photochemical cleavage rate was found to be equal for the two sources, after correcting for the EB extinction coefficient. Photocleavage rates have been calculated from the fraction of uncleaved DNA. If I_- is the quantity of full-length DNA prior to irradiation and I_+ is that of the irradiated sample, the ratio I_+/I_- becomes the fractional change in the number of full-length molecules due to irradiation, which is related by Poisson statistics to the average number (N) of cuts per strand: $I_+/I_- = \exp(-N)$ where N is a product of n, the average number of ethidium molecules bound per strand, and p is the probability of cleavage (the cutting efficiency) per bound EB molecule (Boles & Hogan, 1984). In general, p is a function of intensity, wavelength, and time. Other parameters held constant, the time dependence of cleavage can be expressed as a first-order rate equation: $p(t) = p_0[1 - \exp(-kt)]$ where k is the apparent first-order rate constant for the light-induced process and $p(t)$ and p_0 are the cutting efficiency at irradiation times equal to t and infinity, respectively. (B) EB bleaching kinetics. A 146 bp complex was prepared as above, at 1 EB equiv per 15 bp. Irradiation was performed as above. After irradiation, EB absorbance was measured on a HP 4050 dual-beam spectrophotometer after dissociating the dye–DNA complex by dilution into a 1:1 DMSO/water mixture.

standard conditions of irradiation, intensity, and wavelength, the overall reaction rate is determined to be 0.32 single strand cut/min (Figure 1A).

We have measured a similar rate and photochemical end point, at 4, 20, and 47 °C, with a 219 bp *Crithidia fasciculata* DNA fragment prepared as in the legend to Figure 4 (Table I). This suggests that the EB photocleavage reaction is not measurably dependent on temperature or the sequence of the DNA substrate.

Table I: Properties of EB-Mediated DNA Photochemistry

	temp (°C)		
	4	20	47
(A) Cleavage Rate Constants (Cuts EB^{-1} min^{-1})[a]			
146 bp	0.25	0.32	0.2
219 bp DNA	0.3	0.3	0.4
pUC13 plasmid		0.3	
(B) Cleavage End Point (Cuts/EB)[b]			
146 bp	0.9	1.0	0.8
219 bp DNA	1.1	0.8	1.1
pUC13		1.0	
pUC13 + 25 mM azide		1.0	

(C) Strand Break Mechanism[c]	mobility	bases/bound EB
TLC base species #1	1	0.25
TLC base species #2	0.6	0.06

(D) ^{32}P Labeling of EB Cleavages[d]	^{32}P equiv/nick
DNase I mediated brakes	1
EB-mediated brakes	1.3 ± 0.2

[a] Photocleavage kinetics were measured for 146 bp DNA and the 219 bp *Bam*HI fragment as described in the legend to Figure 1, at 1.7 added EB equiv per strand. DNA concentration was held constant at 5×10^{-4} M bp. Temperature during irradiation was maintained by a regulated flow of argon. For 146 bp DNA, strand breakage was analyzed on a 6% acrylamide/8 M urea gel. For the 219 bp fragment, analysis was on a 2% agarose gel in 30 mM NaOH/1 mM EDTA. For closed-circular pUC13 (2 EB per plasmid equiv), cleavage was analyzed on a native 1% agarose gel, taking advantage of the fact that, if photocleavage occurs randomly, the fraction of closed to nicked circles is given by (closed/nicked) = $\exp(-N)/[1 - \exp(-N)]$ where N is the average number of breaks per plasmid molecule. [b] The cleavage rate and end point in each class of analysis were determined by fitting of the data to the exponential relation in Figure 1. [c] As previously suggested (Deniss & Morgan, 1975), base liberation during EB photochemistry was determined by ascending silica gel TLC, employing 1:9 ammonium acetate/ethanol as the solvent system. For these measurements, the plasmid pUC13 was nicked-translated with ^{3}H-labeled dGTP and purified (the other three nucleotides were administered cold). DNA concentration was then raised to 5×10^{-4} M by addition of unlabeled 146 bp DNA, and EB was added to $^1/_{50}$th base equiv (the buffer was 10 mM Tris-HCl/1 mM EDTA, pH 7.8). DNA was then irradiated to the photochemical end point as in Figure 1. Photolysis products were chromatographed with ^{3}H-labeled guanine and dGMP as standards. The chromatograms were analyzed by scintillation counting. Relative mobilities of the two resulting ^{3}H-labeled photoproducts have been normalized to that measured for the guanine standard. The fraction of total guanine which was liberated as each of the two photoproducts was determined from the ^{3}H activity associated with each chromatographic species, relative to thaat of high molecular weight DNA (which remains at the origin in this TLC assay system). The fraction of guanine liberated per bound EB was generated by normalizing to the EB binding density (1 per 50 bases). [d] The chemical structure of the termini generated by EB-mediated photochemistry was probed by their capacity to be ^{32}P labeled with polynucleotide kinase. A 6.2-kb supercoiled plasmid pHMX (Boles & Hogan, 1987) was subjected to controlled pancreatic DNase I digestion to produce 1.3 single strand breaks per plasmid (as assessed from the ratio of nicked to closed circles) followed by phenol extraction, ethanol precipitation, and drying. The supercoiled plasmid pUC8 (2.7 kb) was then nicked by EB photochemistry to 1.8 single-strand breaks per plasmid (measured as above) followed by treatment with calf intestinal alkaline phosphatase, two phenol extractions, ethanol precipitation, and drying. The two nicked plasmids were then resuspended and mixed so that the concentration of DNase I mediated and EB-mediated termini was equal. The mixture was then treated with polynucleotide kinase and [γ-^{32}P]ATP under standard conditions. The reaction was quenched with EDTA, and the products were analyzed immediately by EB fluorescence and by autoradiography on a native 1% agarose gel. Because of the plasmid size difference, all four plasmid species are cleanly resolved on a single gel profile of that kind. Under standard conditions, we found that the ^{32}P-labeling procedure did not itself produce strand breaks in these plasmids (as assessed by the ratio of closed to nicked circles after fluorescence staining). Polynucleotide kinase labeling efficiency was determined by densitometry of the resulting autoradiograms. The ^{32}P-labeling efficiency for a DNase I-mediated strand break was arbitrarily assigned a value of 1.

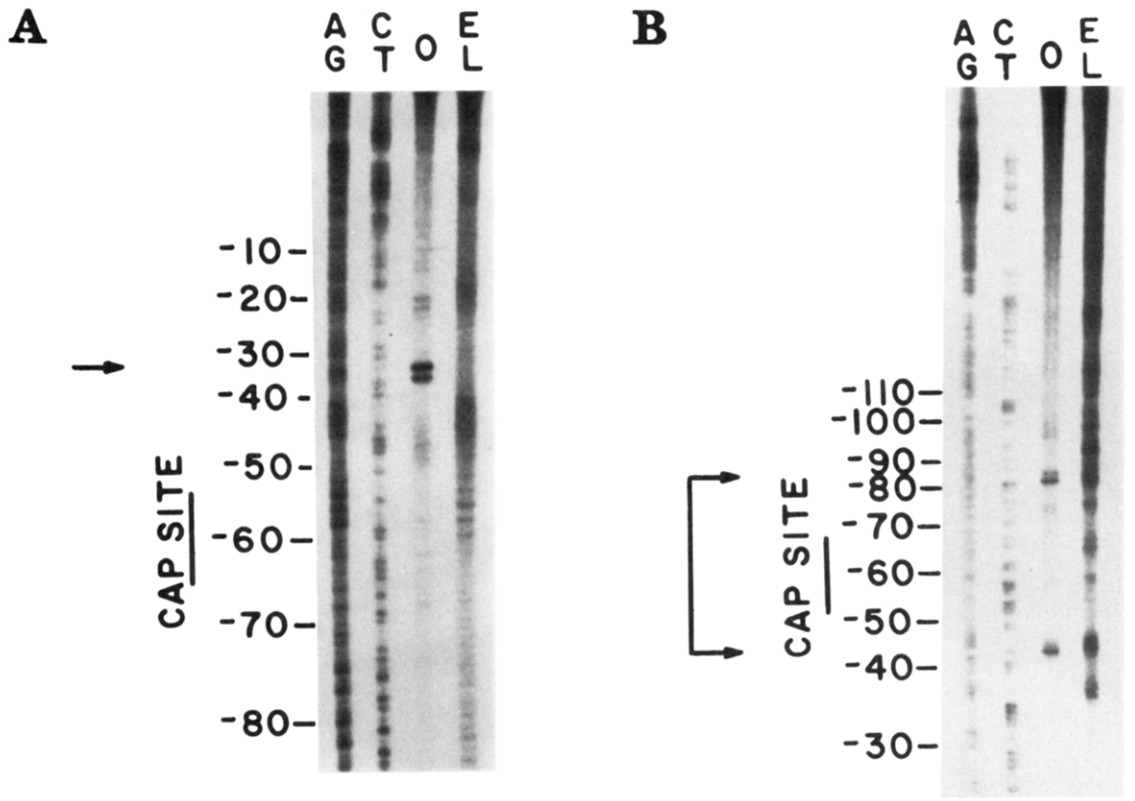

FIGURE 2: Mapping of EB photocleavage sites within a random sequence. Plasmid pUC13 was digested with *Hin*dIII or *Hin*fI, 3′ end labeled with Klenow polymerase, and then digested secondarily with *Hin*fI (A) or *Hin*dIII (B), respectively. The resulting 129 bp fragment was deproteinized and purified by electroelution followed by concentration and chromatography over a Sephadex G100 column to remove contaminants. DNA concentration was adjusted by adding unlabeled 146 bp DNA as a carrier to 5×10^{-4} M bp. Ethidium was then added to a density of 1 per strand (1 per 129 base equiv overall). Irradiation was performed as described in Figure 1A, for 10 min to ensure that the photochemistry had been pushed to the end point. Samples were then diluted 4/1 with deionized formamide, denatured by heating to 70 °C for 3 min, and then loaded directly onto a denaturing 8% acrylamide/0.5% bis(acrylamide) sequencing gel and run at 65 °C. Cleavage was detected by autoradiography (lane labeled EL) relative to ^{32}P-labeled products of DMS or hydrazine sequencing chemistry (lanes labeled AG and CT) within the same region. Lane 0 represents a photochemical control which had been irradiated in the absence of EB. The arrows to the left of the profile identify a spurious enzyme cleavage site which is present in the unirradiated starting material. The contribution of this species is subtracted away in the photocleavage distribution of Figure 3.

The cleavage process has also been assayed on plasmids by monitoring the nicking of covalently closed circular DNA (Table I). At 2 EB bound per plasmid, only nicked circles are detected, which confirms that ethidium photochemistry produces single-strand breaks.

Quantitation of EB photocleavage on plasmids suggests that the cleavage rate and end point are identical with those for 146 bp DNA (Table I). Since plasmid cleavage analysis did not require DNA denaturation by base or heat, the data require that, once irradiated, the subsequent cleavage events occur spontaneously at room temperature and neutral pH.

The EB absorption spectrum during the course of the cleavage reaction is displayed in Figure 1B. A decreasing absorbance maximum at 505 nm and a corresponding increase in absorption at 430 nm reflect an apparent two-state photochemical bleaching process with a time dependence which parallels that of the cleavage reaction. As we have discussed previously for BPDE photochemistry, such temporal correspondence is consistent with the idea that dye bleaching and DNA cleavage are directly coupled (Boles & Hogan, 1984).

EB-mediated photocleavage has been reported to depend on dissolved oxygen (Deniss & Morgan, 1975). That O2 dependence could mean that the cutting process is mediated by singlet oxygen (*O2) which is sensitized by triplet-state EB (Hogan et al., 1987). However, that formal possibility is unlikely because ethidium has an unmeasurably low triplet yield (unpublished results from our laboratory) and because EB-mediated strand breakage does not require treatment with strong base (Table I), as is generally the case for *O2-mediated chemistry (Friedman & Brown, 1978).

To rule out the involvement of diffusible *O2 more explicitly, ethidium photocleavage was measured in the presence of the potent singlet oxygen quencher sodium azide. Since the cleavage rate did not change at a quencher concentration as high as 25 mM (Table I), it is certain that EB photocleavage is not mediated by diffusional *O2 (Hasty et al., 1972).

The data at hand are not sufficient to rigorously define the EB photochemical cutting mechanism in molecular detail (nor is a detailed model required for the mapping analysis below). Nevertheless, it is useful to consider a working hypothesis which is consistent with the data of Table I and with the mechanistic analysis of Deniss and Morgan.

As Deniss and Morgan have proposed, EB abstracts hydrogen from a deoxyribose sugar moiety at the binding site, thereby generating an unstable furanose radical which adds oxygen to form a peroxide which then decomposes in a reaction leading to oxidative cleavage of the phosphate backbone. Direct photochemistry of that kind usually occurs from the triplet. However, since the ethidium singlet is long lived (25 ns when intercalated) and the quantum yield for the cleavage reaction is relatively low, we feel that singlet-state chemistry is reasonable in this instance.

An intact 5′ terminus and a disrupted nucleotide at the 3′ terminus would be produced as a result of the EB-sensitized radical chemistry proposed by Deniss and Morgan (1975). That proposed mechanism is supported by two experimental

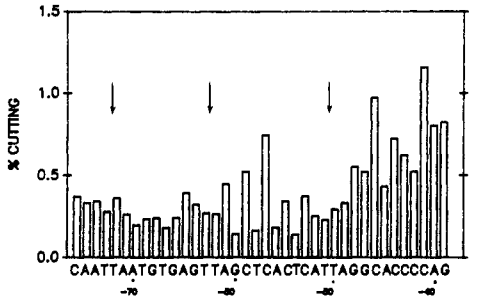

FIGURE 3: EB photocleavage distribution within a random sequence. Autoradiograms as in Figure 2 have been quantified by densitometry. The optical density of the fragment distribution was integrated between 2 and 128 bases and is used as a measure of the total EB-mediated photocleavage. When a photocleavage distribution is normalized by that integrand, it has dimensions of percent cleavage vs position and can be compared to similarly normalized data from another experiment or from the complementary DNA strand. The sum of the photocleavage distributions on the two strands of the helix (bars in Figure 3) is equivalent to the distribution of EB photocleavage within this region and, because the photocleavage is stoichiometric, approximates the EB binding affinity distribution (see text). Numbering is relative to the mRNA start site in the lac Z gene. The sequence of the coding strand is displayed on the *x* axis. A subset of the mapping data has been displayed in which the EB photocleavage distribution could be monitored on both strands at one-base resolution. Arrows refer to sites with ApA nearest neighbors.

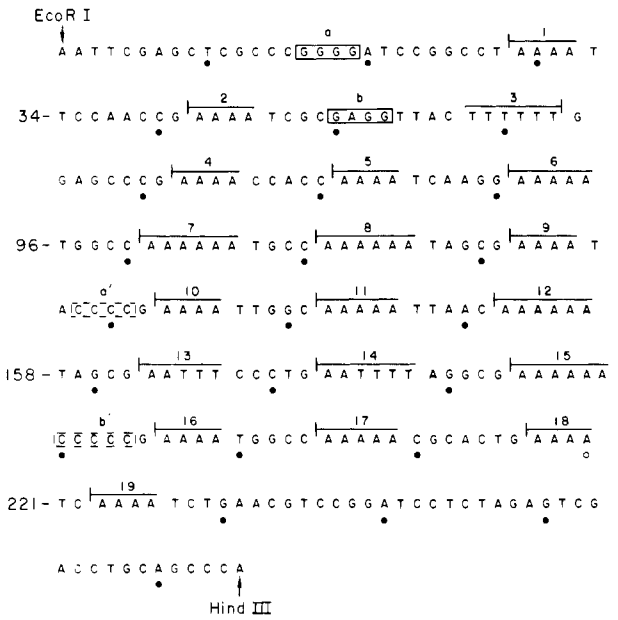

FIGURE 4: Sequence of a "bent" DNA fragment from *C. fasciculata*. We have displayed a 265 bp *Eco*RI–*Hin*dIII fragment of *C. fasciculata* DNA which was cloned to form the plasmid pPK201/CAT by Englund and colleagues (Kitchin et al., 1986). Numbering is relative to the 5′ *Eco*RI terminus. Oligo(A) tracts have been identified with numbered bars which have been marked with a vertical tick at the 5′ end of the oligo(A) sequence. This graphical symbolism is used in subsequent figures. C-rich polypyrimidine stretches are indicated by broken boxes with the labels a′ and b′. G-rich polypurine sequences are identified by solid boxes.

observations: (i) The nature of the 5′ terminus of an ethidium-nicked plasmid DNA was determined by quantitative kinase labeling relative to that of DNase I cleavage sites (Table I). Incorporation of label at photochemical cleavage sites was found to be 1.3 times that at DNase I sites, which suggests that EB photocleavage results in a relatively intact 5′ terminus. (ii) Thin-layer chromatography of EB-mediated photocleavage products reveals that free guanine base and a guanine derivative have been liberated by the photochemistry in the ratio 3 to 1 (Table I), suggestive of chemical alteration of the nucleotide which comprises the 3′ terminus of the cleavage site.

Clearly, the detailed structure of the nascent termini cannot be elucidated from the preliminary data presented here. However, even in the absence of those mechanistic details, it is clear from the data presented above that, on average, the photocleavage produces one DNA strand break at each EB binding site. As such, the distribution of those photocleavages can be used to estimate the EB binding affinity distribution on a DNA fragment.

Ethidium Binding to Random-Sequence DNA. We have examined the distribution of EB photocleavage within a region of the *Escherichia coli* lactose operon, 38 nucleotides upstream from the mRNA start site, which includes the CAP protein binding domain. This region comprises a nearly random DNA sequence which can be used to compare the microscopic EB photocleavage distribution with the EB base sequence preference which had been inferred previously from equilibrium binding data (Kastrup et al., 1972; Baguley & Falkenhaug, 1978).

EB photocleavage sites were mapped by high-resolution electrophoresis, at a bound density of 1 EB per 129 bases (Figure 2). Autoradiograms of such gels were quantified by densitometry and the resulting cleavage patterns expressed as the total photocleavage likelihood vs position (see Figure 2 for details of the data handling).

Inspection of Figure 3 reveals that, as expected from traditional binding analysis, the total EB photocleavage distribution is relatively uniform in this random-sequence domain, with a moderate preference for nearest-neighbor sites with one or more GC base pairs. As will be evident below, it is also important to note that, as equilibrium binding analysis had predicted (Kastrup et al., 1978; Baguley & Falkenhaug, 1978), the likelihood of EB photocleavage between isolated ApA nearest neighbors in this region is not significantly different than the average (ApA sites are marked by arrows in Figure 3).

Close inspection of the raw cleavage data in Figure 2A, reveals that the photochemical cleavage at an intercalation site is directed toward purine residues, with negligible cutting at the pyrimidine residue on the complementary strand.

We tentatively attribute such asymmetry to stacking between EB and adjacent bases within the dinucleotide binding site, i.e., as suggested by the available crystallography of intercalation complexes (Tsai et al., 1977), perfect 2-fold symmetry of an intercalation complex will be lost in the process of optimizing base stacking between EB the purine bases at the binding site. The effect is expected to be most pronounced at Pu-Pu dinucleotides.

EB Photocleavage within a "Bent" DNA Domain. DNA fragments with repetitive oligo(A) domains have been widely studied, because of aberrant structural properties which have been ascribed to an unusual structural state assumed by the oligo(A) element (Koo et al., 1986; Marini et al., 1984; Ulanovsky & Trifanov, 1987). Here, we apply the EB photocleavage method to analyze DNA structure variation within a natural example of such an oligo(A) motif.

The plasmid pPk201/CAT containing a 265 bp fragment of *C. fasciculata* DNA was linearized with restriction endonuclease *Eco*RI, ^{32}P-labeled at its *Eco*RI site as described in the legend to Figure 5, and then cleaved with *Hin*dIII to liberate a singly labeled 265 bp DNA segment [see Figure 4 for its sequence, as determined by Kitchin et al. (1986)].

EB was added to a final bound density between 0 and 4 bound equiv/strand and then irradiated to the photochemical end point at either 4 or 47 °C. Photocleavage products were

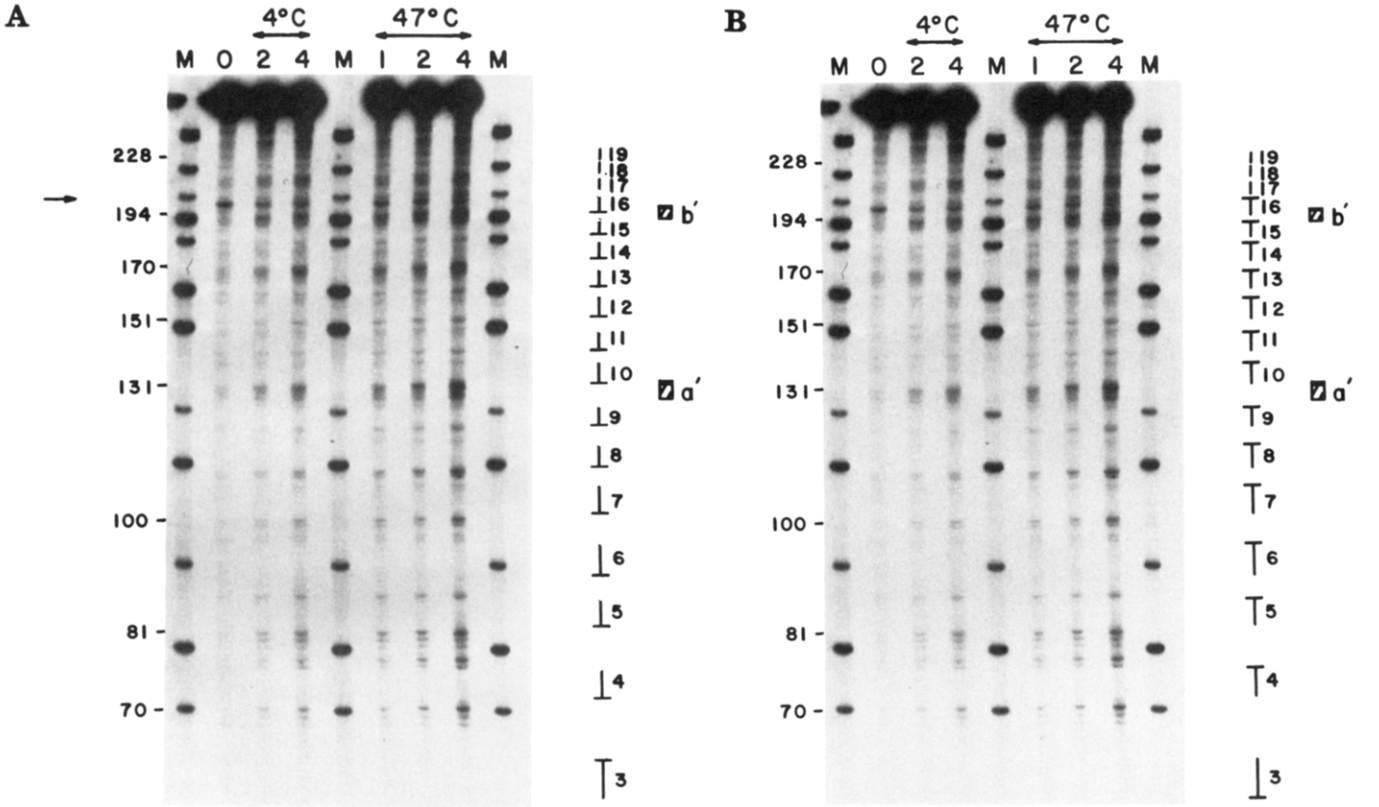

FIGURE 5: Mapping of EB photocleavage sites in a "bent" DNA fragment. pPK201/CAT was digested with *Eco*RI and then either 3′ labeled with Klenow polymerase or 5′ labeled by treatment with alkaline phosphatase and polynucleotide kinase. Labeled DNA was then cleaved with *Hin*dIII and isolated from the plasmid vector by chromatography over a 10-cm Sepharose 2B column. Unlabeled 146 bp DNA was added to 5×10^{-4} M as a carrier, and EB was added as needed to a final density between 1 and 4 per strand (the lane labeled 0 represents an irradiated control without added EB). Photocleavage was carried out as described in Figures 1 and 2 at either 4 or 47 °C and analyzed on a standard 8% acrylamide sequencing gel. Cleavage position was determined relative to the equivalently labeled *Hpa*II digest of pBR322 (lane marked M in Figure 5B). The length of prominent photocleavage sites is marked to the left, in the numbering system of Figure 4. Numbered bars to the right correspond to the position of oligo(A) tracts in the fragment profile. The 5′ end of each oligo(A) tract is identified by a horizontal tick. The hatched boxes (a′ and b′) correspond to polypyrimidine stretches. Autoradiograms A and B correspond to mapping data relative to the 5′ and 3′ *Eco*RI terminus, respectively. The arrow to the left corresponds to a spurious enzymatic cleavage site which is present in the unirradiated DNA starting material. Its contribution to the EB-mediated cleavage profile has been subtracted in the subsequent analysis.

denatured by heating in formamide and visualized on a standard 8% sequencing gel (Figure 5A,B). In Figure 4 and throughout, we have identified oligo(A) segments by a numbered bar, with one end marked to signify the 5′ end of the oligo(A) stretch.

Autoradiograms were quantified by densitometry. As for the CAP domain, we have summed the EB photocleavage distribution on each of the two strands in this region. The resulting distribution of total photocleavage has been presented in Figures 6 and 7, normalized to averaged cleavage likelihood within the repeated oligo(A) motif.

For the purpose of clarity and as suggested by the mechanistic analysis described above, we assume that this summed distribution is essentially equivalent to the distribution of EB binding affinity within the "bent" DNA fragment.

Examination of that EB photocleavage (binding affinity) distribution reveals several general features.

Oligo(A) Segments Bind EB Very Poorly. This effect confers a distinct striated appearance to the autoradiograms (Figure 5). In Figure 6A,B, we have used arrows to identify isolated ApA dinucleotide elements which are outside an oligo(A) domain. As a class, and as expected from EB binding to the random-sequence CAP domain, isolated ApA elements in the fragment bind EB with approximately 5-fold higher affinity than when part of an oligo(A) array.

Previously, Baguley and Falkenhaug have used equilibrium binding isotherms to show that the synthetic duplex poly(dA)·poly(dT) displays EB binding affinity which is approximately one-tenth that of its sequence isomer poly[d(AT)]·poly[d(AT)] or random DNA sequences (Baguley & Falkenhaug, 1978). As they have noted, reduced EB binding affinity to that synthetic polymer may result from the atypical secondary structure which is adopted by the poly(dA)·poly(dT) duplex (Arnott et al., 1983; Nelson et al., 1987).

The uniform reduction of EB binding affinity which we have seen in the *C. fasciculata* fragment suggests that oligo(A) tracts have assumed a secondary structure with the same low EB binding affinity measured for poly(dA)·poly(dT). By the same argument, ApA segments in isolation do not display that unusual binding property. Using a DNase I footprinting technique, Fox and Waring have shown that a 4 °C, EB did not alter DNase I cleavage within oligo(A) segments of the tyrT gene (Fox & Waring, 1987). On the basis of that observation, they concluded that EB binds weakly to oligo(A) tracts within an otherwise random DNA sequence (Fox & Waring, 1987).

As such, the direct photochemical mapping data which we have presented are consistent with their interpretation of the DNase I footprinting data.

On the basis of crystallographic analysis of an oligonucleotide duplex, Klug and colleagues have determined that oligo(A) domains adopt a secondary structure with propeller-twisted base pairs and an unusually narrow minor groove (Nelson et al., 1987). Relative to the canonical B form, those characteristic DNA structure features might be expected to resist the minor groove access (Tsai, 1977) and base plane

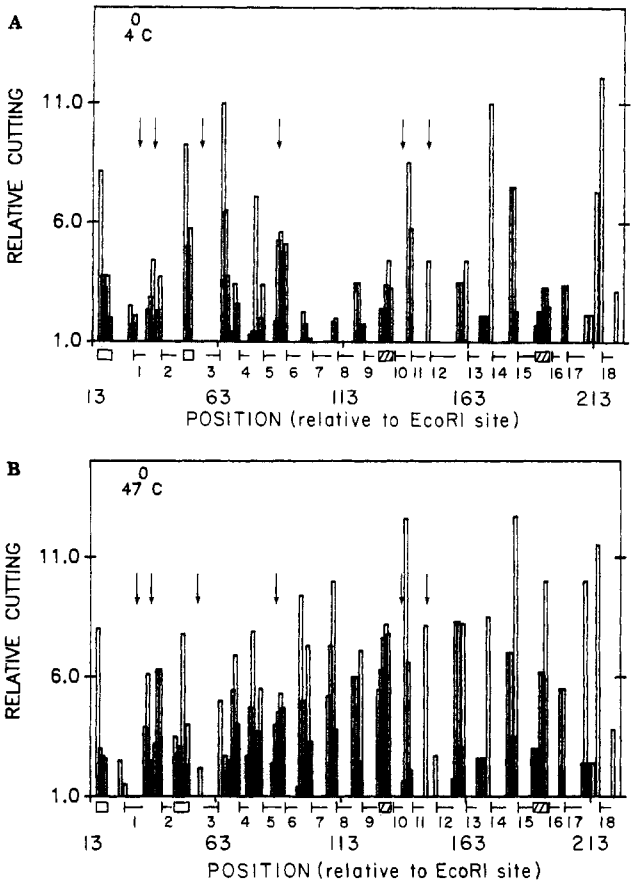

FIGURE 6: EB photocleavage distribution within a bent DNA fragment. EB photocleavage within the 265 bp *Eco*RI–*Hin*dIII fragment has been calculated by summing the normalized EB photocleavage profile on both strands, as in Figure 3. To emphasize the relation to cleavage within the oligo(A) segments, the average cleavage likelihood in those regions has been assigned a value 1; i.e., the vertical bars in Figure 3 are a measure of photocleavage likelihood, relative to that within the oligo(A) elements. The numbering is relative to the *Eco*RI terminus. Horizontal bars correspond to oligo(A) tracts as in Figure 4. Vertical arrows identify ApA dinucleotides in the fragment which are not part of a contiguous oligo(A) tract. Panels A and B are the distributions calculated from EB photochemistry at 4 and 47 °C, respectively.

flattening (Tsai et al., 1977; Hogan et al., 1979) required for EB binding and, consequently, may be the features which best explain why EB binding affinity within the oligo(A) domain is so low.

EB Appears To Be Attracted to the Structural Interface Formed at the Ends of Most Oligo(A) Segments. A second prominent feature of ethidium binding to the kinetoplast is that the interface formed at the two ends of an oligo(A) tract binds EB more tightly than an equivalent dinucleotide sequence in isolation. Such interfacial binding is evident in the autoradiograms in Figure 5A,B and in the numerical profiles in Figure 6. As a class, 9 of the 14 junctions which can be modified at high resolution display a "saddleback" EB binding pattern: high-affinity binding at the interface with an adjoining oligo(A) segment, with more ordinary binding affinity near the center of the junction. If identified by their position relative to the two adjacent oligo(A) elements, it can be seen that junctions 1/2, 3/4, 4/5, 6/7, 7/8, 8/9, 11/12, 12/13, and 13/14 fall into this category.

To emphasize that those junctional domains comprise a class of EB binding site, we have averaged the EB photocleavage distribution within those nine junctional sites and have presented the average in Figure 7, along with error bars which represent 1 SD, from the mean of the nine measurements. Data have been presented as average cleavage likelihood vs position in the junction, as a fraction from 0 to 1 to correct for differences in junction length (0 is the 5′ end, 1 is the 3′ end of the junction). Although the "saddleback" binding pattern is well-defined with respect to position in the junctional domain ($p < 0.05$), we do not detect a simple sequence dependence to the patterns. Therefore, we conclude that EB binds to this set of oligo(A) interfaces with high affinity because of unique physical properties common to this interfacial site and not because of sequence features within the junction.

On the basis of crystallographic analysis, Klug and colleagues have suggested that each end of such a oligo(A) segment assumes a distinct interfacial structure (Nelson et al., 1987), the junction at the 5′ end being characterized by a bend which opens the major helix groove (negative roll) while the 3′ junction is characterized by bending which opens the minor groove (positive roll).

Crystallographic analysis of EB binding has shown that EB intercalates into DNA by access through the helix grooves, displaying a preference for minor-groove binding (Tsai et al., 1975). A variety of less direct methods have suggested that the intercalation process might be favored by unstacking of a helix (a local increase of helix roll) which facilitates entry into the helix through the grooves (Hogan et al., 1987; Kean et al., 1975).

In that context, it is reasonable to consider that the junctions at either end of an oligo(A) tract bind EB with high affinity because of the unstacked cleft which may be formed there.

In the other four oligo(A) junctions which can be studied at high resolution (2/3, 5/6, 9/10, 10/11), ethidium binding does not appear to be characterized by high-affinity binding at the oligo(A) interfaces. Instead, the individual binding distributions within each of the four are characterized by ordinary to low-affinity ethidium binding at the interface, with high-affinity binding at one or more sites elsewhere in the junction. The averaged photocleavage pattern within those sites is presented in Figure 7B.

On the basis of those four exceptions to the "saddleback" EB binding pattern, we must conclude that in certain instances, as yet unknown sequence effects can contribute to the interfacial binding properties of EB.

EB Photocleavage within the Oligo(A) Segment Is Not Significantly Temperature Dependent. Gel electrophoresis has shown that the characteristically slow mobility of a fragment with phased oligo(A) segments becomes nearly indistinguishable form that of a random DNA sequence at 47 °C, which has been interpreted as temperature-induced straightening of the helix (Diekmann & Wang, 1985). We have confirmed those gel observations with preparations of the 265 bp *C. fasciculata* fragment used in this study (unpublished data).

Figure 5A,B contains cleavage data which compare the EB binding distribution at 4 and 47 °C. The temperature dependence of the binding distribution is presented graphically by comparison of Figure 6A,B and 7. At the first level of interpretation, the data show that the pattern of EB binding seen at 4 °C persists at 47 °C, i.e., EB binds poorly within the oligo(A) domain and with high affinity to junctional regions at either temperature, although subtle changes can be detected within the junctional domains (Figure 7).

That observation poses a dilemma, because it suggests that the apparent straightening of a phased oligo(A) array, as detected by electrophoresis, occurs independently of a DNA state change within the oligo(A) segment, as detected by the heterogeneous pattern of EB binding affinity.

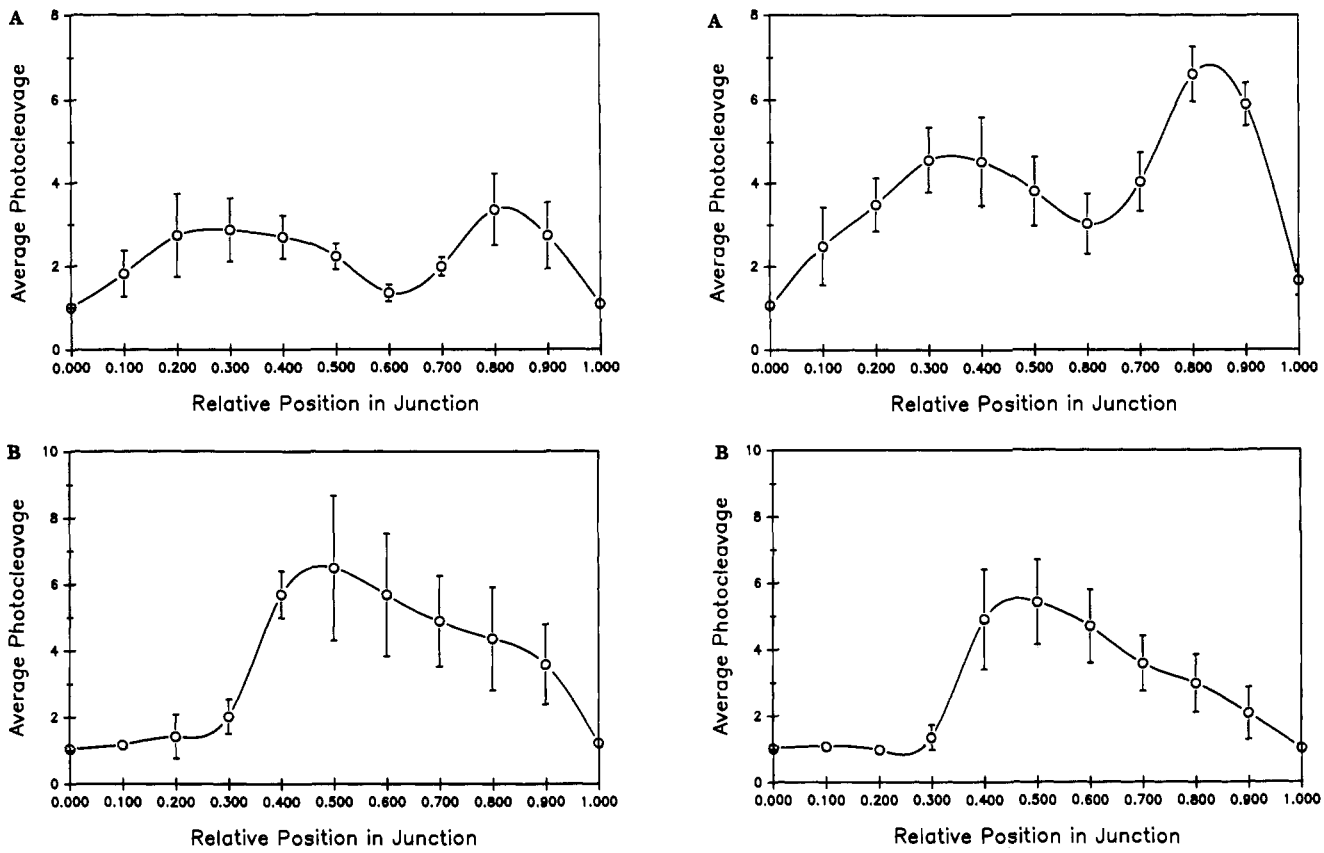

FIGURE 7: EB photocleavage distribution within junctional regions. The data of Figure 6 have been expanded, to display the EB photocleavage distribution within the DNA which connects oligo(A) segments. Junctional domains have been identified by the number associated with the flanking oligo(A) segments, as defined in Figure 4. As discussed in the text, the junctions appear to fall into two general classes: 1 (panels A) (1/2, 3/4, 4/5, 6/7, 7/8, 8/9, 11/12, 12/13, 13/14) and 2 (panels B) (2/3, 5/6, 9/10, 10/11). To emphasize the similarity among elements, we have averaged the EB photocleavage distribution among members of each set and have presented the averages. Data have been presented as average cleavage likelihood vs position in the junction, as a fraction from 0 to 1 to correct for differences in junction length (0 is the 5′ end, 1 is the 3′ end of the junction). (Left panels) Binding data accumulated at 4 °C. (Right panels) Binding data at 47 °C. The vertical scale of these plots is identical throughout. Data are normalized such that EB photocleavage within an internal random-sequence domain (positions 19–38 in Figure 4) was assigned a value of 1. Therefore data in Figure 7 have the dimension of photocleavage likelihood, relative to an internal random-sequence standard. Error bars are 1 SD from the mean of the data sets which comprise sets 1 and 2.

That apparent inconsistency cannot be resolved by the data which we have presented. However, the inconsistency is independent of the structure model which is used to interpret the EB mapping data, and should be taken seriously.

Conclusions

Photochemical Mapping Technique Has Several Practical Advantages. Others have devised elegant methods to map EB binding sites on DNA: the addition of metal catalysts to the EB analogue MPE (Van Dyke & Dervan, 1982) and footprinting of EB binding sites with DNases (Fox & Waring, 1987).

In general, a consistent model for EB binding specificity has not yet been inferred from those indirect mapping techniques:

Mapping of MPE cleavage sites has led Dervan and colleagues to conclude that intercalation occurs randomly with respect to DNA sequence (Van Dyke & Dervan, 1982). With DNase II footprinting, or DNase I footprinting at 37 °C, Fox and Waring have detected little or no apparent site specificity for EB binding but (within the same *tyr*T DNA region) have inferred significant EB binding specificity from footprinting with DNase I at 4 °C (Fox & Waring, 1987).

Fox and Waring suggest that the inconsistency evident in indirect EB mapping experiments may be due to DNA structure specificity of the chemical or enzyme which is being used to detect EB binding, or to lifetime effects; i.e. to be detected, its bound lifetime must be long relative to the forward rate constant for the (secondary) chemical or enzymatic cleavage process.

Because the EB photochemistry results from direct interaction between bound EB and the helix and because the cleavage reaction is stoichiometric, rather than catalytic, under standard assay conditions, the photochemical technique presented here may obviate much of the ambiguity associated with previous mapping techniques.

Consequently, raw EB mapping data (a strand break distribution on a gel) converge to the intercalator binding site distribution of interest and are not sensitive to probe-related artifacts such as those which have been discussed by Fox and Waring.

A second practical advantage of the EB photochemical mapping technique is related to the efficiency of the cleavage reaction. EB photocleavage can be mapped at a very low bound density, the sensitivity of the method being limited by the presence of uncontrolled cleavage processes (stray enzymatic cleavages, metal-catalyzed oxidation during heating steps, etc.) which under standard conditions specifies a useful limit of 1 bound EB per 2000 base equiv. We believe that measurements at such a low bound density will circumvent many of the artifacts which can arise from binding site saturation, as during a footprinting analysis or analysis by an inefficient chemical method.

EB Binding May Provide Insight into Rare, High-Affinity Binding Sites within Genes. Equilibrium binding analysis has

hinted that a genome may possess very high affinity intercalator binding sites (Winkle et al., 1982). The photochemical method described in this paper provides a technique to search for such rare sites in a direct way, at biologically meaningful bound density (less than 1/100 bases) and then evaluate structure/binding relationships at such sites in terms of discrete molecular models.

Registry No. EB, 1239-45-8.

References

Arnott, S., Chandrasekharan, R., Hall, I. H., & Puigjaner, L. C. (1983) *Nucleic Acids Res. 11*, 4141–4155.

Baguley, B. C., & Falkenhaug, E. (1978) *Nucleic Acids Res. 5*, 161–171.

Boles, T. C., & Hogan, M. E. (1984) *Proc. Natl. Acad. Sci. U.S.A. 81*, 5623–5627.

Boles, T. C., & Hogan, M. E. (1986) *Biochemistry 25*, 3039–3043.

Boles, T. C., & Hogan, M. E. (1987) *Biochemistry 26*, 367–376.

Burkoff, A. M., & Tullius, T. D. (1987) *Cell 48*, 935–943.

Deniss, I. S., & Morgan, A. R. (1975) *Nucleic Acids Res. 3*, 315–323.

Diekmann, S., & Wang, J. C. (1985) *J. Mol. Biol. 186*, 1–11.

Drew, H. R., & Travers, A. A. (1984) *Cell 37*, 491–502.

Felsenfeld, G. (1986) *Sci. Am. 253*, 58–67.

Fox K. R., & Waring, M. J. (1987) *Nucleic Acids Res. 15*, 491–507.

Friedman, T., & Brown, D. M. (1987) *Nucleic Acids Res. 5*, 615–622.

Hasty, N., Merkel, P. B., Rodlick, P., & Kearns, D. R. (1972) *Tetrahedron Lett. 1*, 49–55.

Hogan, M. E., Rooney, T. R., & Austin, R. H. (1987) *Nature 328*, 554–557.

Hogan, M. E., Dattagupta, N., & Crothers, D. M. (1979) *Biochemistry 18*, 280–288.

Johnston, B. H., & Rich, A. (1985) *Cell 42*, 713–724.

Kastrup, R. V., Yound, M. A., & Krugh, T. R. (1978) *Biochemistry 17*, 4855–4876.

Kean, J. M., White, S. A., & Draper, D. E. (1985) *Biochemistry 24*, 5062–5070.

Kitchin, P. A., Klein, V. A., Ryan, K. A., Gann, K. L., Rauch, C. A., Kang, D. S., Wells, R. D., & Englund, P. T. (1986) *J. Biol. Chem. 261*, 11302–11309.

Koo, H. S., Woo, H. M., & Crothers, D. M. (1986) *Nature (London) 320*, 501–506.

Kowhi-Shigematsu, T., Gelinas, R., & Weintraub, H. (1983) *Proc. Natl. Acad. Sci. U.S.A. 80*, 4389–4393.

Leslie, A. G. W., & Arnott, S. (1980) *J. Mol. Biol. 143*, 49–72.

Marini, J. C., Effron, P. N., Goodman, T. C., Singleton, C. D., Wells, R. D., Wartell, R. D., & Englund, P. T. (1984) *J. Biol. Chem. 259*, 8974–8979.

Mei, H. Y., & Barton, J. K. (1988) *Proc. Natl. Acad. Sci. U.S.A. 85*, 1339–1343.

Muller, B. C., Raphael, A. L., & Barton, J. K. (1987) *Proc. Natl. Acad. Sci. U.S.A. 84*, 1764–1768.

Nelson, J. W., & Tinoco, I., Jr. (1985) *Biochemistry 24*, 6416–6421.

Nelson, H. C. M., Finch, J. T., Bonaventura, F. L., & Klug, A. (1987) *Nature 330*, 221–226.

Saenger, W. (1984) *Principles of Nucleic Acid Structure*, p 350, Springer-Verlag, New York.

Trifonov, E. N., & Sussman, J. L. (1980) *Proc. Natl. Acad. Sci. U.S.A. 77*, 3816–3820.

Tsai, C., Jain, S. C., & Sobell, H. M. (1977) *J. Mol. Biol. 114*, 301–315.

Ulanovsky, L. E., & Trifonov, E. N. (1987) *Nature (London) 326*, 720–722.

Van Dyke, M. W., & Dervan, P. B. (1982) *Proc. Natl. Acad. Sci. U.S.A. 79*, 5470–5474.

Wang, N. C., Hogan, M. E., & Austin, R. H. (1982) *Proc. Natl. Acad. Sci. U.S.A. 79*, 5896–5900.

Winkle, S. A., Rosenburgh, L. S., & Krugh, T. R. (1982) *Nucleic Acids Res. 10*, 8211–8223.